RSC Advances

PAPER

View Article Online
View Journal | View Issue

Cite this: *RSC Adv.*, 2023, **13**, 25930

Fabrication of ACP–CCS–PVA composite membrane for a potential application in guided bone regeneration†

Qiaolin Du,‡[a] Jian Sun,‡[a] Yanyan Zhou,[b] Yadong Yu,[c] Weijing Kong,[b] Chaoqun Chen,[a] Yifeng Zhou,[a] Ke Zhao,[a] Changyu Shao *[b] and Xinhua Gu *[a]

Received 6th July 2023
Accepted 18th August 2023

DOI: 10.1039/d3ra04498j

rsc.li/rsc-advances

The barrier membranes of guided bone regeneration (GBR) have been widely used in clinical medicine to repair bone defects. However, the unmatched mechanical strength, unsuitable degradation rates, and insufficient regeneration potential limit the application of the current barrier membranes. Here, amorphous calcium phosphate–carboxylated chitosan–polyvinyl alcohol (ACP–CCS–PVA) composite membranes are fabricated by freeze–thaw cycles, in which the ATP-stabilized ACP nanoparticles are uniformly distributed throughout the membranes. The mechanical performance and osteogenic properties are significantly improved by the ACP incorporated into the CCS–PVA system, but excess ACP would suppress cell proliferation and osteogenic differentiation. Our work highlights the pivotal role of ACP in GBR and provides insight into the need for biomaterial fabrication to balance mechanical strength and mineral content.

1. Introduction

The barrier membrane of guided bone regeneration (GBR) forms a biological barrier between soft tissue and the bone defect area to prevent faster migrating fibroblasts and epithelial cells from entering the bone defect area, therefore creating a favorable environment for bone tissue growth.[1] They have been widely used for periodontal treatment and oral implants. Previous studies suggested that an ideal GBR membrane should have barrier function, good biocompatibility, biodegradability, and well-matched mechanical properties.[2] However, the current GBR-based technology for bone regeneration, which employs barrier membranes, requires properties to boost osteoblast proliferation and differentiation as well as promote bone deposition.

Natural bone is an organic-inorganic composite mainly consisting of calcium phosphate (CaP) minerals and collagen fibrils.[3] Currently, the CaP minerals (*e.g.*, tricalcium phosphate (β-TCP), hydroxyapatite (HAP), amorphous calcium phosphate (ACP)) and phosphate and borate bioactive glass are widely used as superior bone graft substitutes and as the inorganic component of biomimetic barrier membranes, which have gained attention due to their excellent osteoconductive and osteoinductive properties.[4–10] However, it is challenging to transform these crystalline CaP minerals into the low-crystalline apatite needed for bone formation since they are stable under physiological conditions,[11] and these bioactive glass tends to lead to inhomogeneities and agglomerate formation within composites.[12]

A growing body of evidence shows that the amorphous precursor, *i.e.*, ACP, is a vital transition phase and bears a fundamental role in bone formation. Amorphous calcium phosphate exhibits better osteoconductivity *in vivo* than apatite and higher biodegradability than tricalcium phosphate.[13–15] In addition, ACP, as nano-sized inorganic structural units, can be uniformly dispersed between polymers, improving the strength of polymers.[16–18] Because the ACP is unstabilized and readily nucleation in an aqueous solution, a stabilizer is required in preparing the stabilized ACP. Polyacrylic acid (PAA), poly aspartic acid (pAsp), and other polyelectrolytes, for example, are used to stabilize the ACP through cation binding,[19] but these polymers may have potential toxicity for cells.[20] The biomolecule adenine nucleoside triphosphate (ATP) is biosafety. It can significantly stabilize the ACP, but the effect of the formed composite on the cell behavior, such as adhesion, proliferation, and differentiation, is poorly understood.

Although collagen membranes are widely used in clinical applications due to their high biocompatibility, their mechanical strength is lower, and are susceptible to enzymatic degradation *in vivo*.[21] To some extent, the mechanical properties of these collagen membranes can be improved by calcium phosphate mineralisation or complexation with other biomaterials (*e.g.* nanohydroxyapatite, silicate ceramic), but this also results

[a]*Department of Stomatology, The First Affiliated Hospital, College of Medicine, Zhejiang University, Hangzhou 310003, China. E-mail: guxh@zju.edu.cn*

[b]*Stomatology Hospital, School of Stomatology, Clinical Research Center for Oral Diseases of Zhejiang Province, Key Laboratory of Oral Biomedical Research of Zhejiang Province, Cancer Center of Zhejiang University, Zhejiang University School of Medicine, Hangzhou 310006, China*

[c]*Department of Chemistry, Zhejiang University, Hangzhou, Zhejiang 310027, China*

† Electronic supplementary information (ESI) available. See DOI: https://doi.org/10.1039/d3ra04498j

‡ Qiaolin Du and Jian Sun contributed equally to this work.

in increased brittleness and reduced toughness of the collagen membranes, which is not conducive to clinical manipulation.[22,23] As a result, other natural polymers such as chitosan, hyaluronic acid, silk fibroin, and synthetic polymers such as polylactic acid, polycaprolactone, and polyvinyl alcohol are also commonly used in biological materials.[24–26] In particular, the *N*-acetylglucosamine moiety of chitosan is similar to the glycosaminoglycan in bone extracellular matrix (ECM), which can attract growth factors and proteins to induce new bone regeneration.[27] In addition, the positive charge of chitosan can improve cell adhesion and diffusion to alter cell behavior.[28] Compared to chitosan, its derivative carboxylation chitosan (CCS) has improved antioxidant properties, higher water retention, excellent biodegradability, biocompatibility, and antibacterial activity. However, the mechanical strength of pure CCS is too weak to maintain the osteogenic space. Another polymer, PVA, with high tensile strength, flexibility, elongation at break, and slow degradation properties, gives PVA-based biomaterials the ability to absorb more of the mechanical strain of the muscle/skeleton.[29,30] However, these polymers lack osteoinductivity and cannot provide osteoblasts with an environment conducive to their proliferation and development.

In the present study, a composite membrane consisting of ATP-stabilized ACP, CCS, and PVA was prepared in which the amorphous particles were uniformly distributed throughout the membrane. Incorporating ACP could dramatically improve the mechanical properties of the composite membrane and enhance osteoblast proliferation and differentiation. However, the excess ACP would lead to suppression, indicating that the ACP should be kept within an optimal concentration range first and then the mechanical properties. These findings provide a clue for the manufacture of biomaterials for GBR and further deepen our understanding of ACP and how it affects bone regeneration.

2. Materials and methods

2.1 Preparation of highly stable ACP nanoparticles

$CaCl_2 \cdot 2H_2O$ (Aladdin, Shanghai, China) and ATP (BBI, Shanghai, China) were dissolved in deionized water at room temperature to prepare solution A, and the pH was adjusted to 9.0 with 1 M NaOH (Aladdin, Shanghai, China). Solution B was prepared by dissolving $NaH_2PO_4 \cdot 2H_2O$ (Aladdin, Shanghai, China) in deionized water. Solution B was added to solution A under magnetic stirring, and the pH was maintained at 9.0 and reacted until solution B dropped off. The final solution concentration was 25 mM $CaCl_2$, 25 mM NaH_2PO_4, and 5 mM ATP. The precipitate was centrifuged, washed 3 times with deionized water and 100% ethanol, and dried in a freeze dryer (FreeZone®, Labconco, USA) for 24 hours to obtain ACP nanoparticles.

2.2 Fabrication of ACP–CCS–PVA composite membranes

The composite membrane used in this study was prepared using a freeze–thaw cycle method. CCS (Aladdin, Shanghai, China, 3 wt%) was completely dissolved in deionized water at room temperature. PVA (Aladdin, Shanghai, China, 6 wt%) was completely dissolved in deionized water at 95 °C and then cooled to room temperature. Mixing the two solutions in a volume ratio of 1 : 1, adding a certain mass of ACP nanoparticles, and fully vibrating to prepare composite membranes with 0 wt%, 10 wt%, and 20 wt% ACP named 0 wt% ACP–CCS–PVA, 10 wt% ACP–CCS–PVA, and 20 wt% ACP–CCS–PVA, respectively. Pour the homogeneous mixture into the mold. Then, the sample was sealed and frozen at −20 °C for 8 h and thawed at room temperature for 3 h. The freeze–thaw cycle process was repeated five times. Eventually, the frozen samples were placed in a freeze dryer (FreeZone®, Labconco, USA) and freeze-dried at −60 °C for 20 h before characterization.

2.3 Characterization

2.3.1 Ultrastructure examination. ACP nanoparticles were evenly dispersed in an anhydrous ethanol solution, scooped out with 300-mesh nickel grids, dried in a fume hood, and operated with a TEM (HT7700, Hitachi, Japan) at an accelerated voltage of 100 kV. Selected region electron diffraction (SAED) patterns of ACPs were recorded using high-resolution transmission electron microscopy (HRTEM, JEM-2100F, JEOL, Japan).

The samples were sputter-coated (E-1010, Hitachi, Japan) with AuePd and morphologically characterized by SEM (Ultra-55, Carl Zeiss, Germany), and performed the element analysis by using energy-dispersive spectrometry (EDS).

2.3.2 Fourier transform-infrared spectroscopy (FTIR). ACP nanoparticles, CCS–PVA composite membrane, and ACP–CCS–PVA composite membrane were analyzed by FTIR (Spectrum 400, PerkinElmer, USA). The FTIR spectrum was collected from the wavelength 400–4000 cm^{-1}, with a resolution of 4 cm^{-1} and a total of 20 scans.

2.3.3 X-ray diffraction (XRD). To examine the mineral phase characteristics of each group of samples, ACP nanoparticles, CCS–PVA composite membrane, and ACP–CCS–PVA composite membrane were detected *via* XRD (Rigaku America, Woodlands, TX, USA) under the conditions of CuKα beam, the voltage of 40 kV, current of 20 mA, scanning angle of 2θ from 10° to 70°, and scanning speed of 6° min^{-1}.

2.3.4 Thermogravimetric analysis (TGA). TGA (SDTQ 600, USA) was performed from approximately 20 °C to 600 °C at a heating rate of 10 °C min^{-1} to determine the inorganic content of CCS–PVA composite membrane, 10 wt% ACP–CCS–PVA composite membrane, and 20 wt% ACP–CCS–PVA composite membrane.

2.3.5 Degradation evaluation *in vitro*. For evaluation of degradation, the composite membrane ($n = 3$; 1 × 1 × 0.5 mm) was soaked with 0.5 mg per mL lysozyme (Sigma-Aldrich, St Louis, MO, USA) in 10 mM PBS (pH = 7.4). The samples were incubated in a sterile incubator at 37 °C, and the new buffer solution was replaced every three days. At different detection time points, samples were removed from the buffer solution, washed with deionized water, and weighed after freeze-drying. The degradation degree (D) was calculated as follows: $D = ((W - W_0)/W_0) \times 100\%$, where W_0 represents the initial mass of different composite membranes, and W represents the mass after 7, 14, 21, 28 days of *in vitro* degradation.

2.3.6 Inductively coupled plasma optical emission spectrometry (ICP-OES) testing. The composite membranes of each group were immersed in physiological saline for 0.17, 1, 3, 5, 7, and 14 days, and the supernatant (0.5 mL) was extracted for ICP-OES (JY 2000-2, Horiba, France) to determine the concentrations of calcium and phosphate ions.

2.3.7 Evaluation of mechanical properties. The dumbbell-shaped and dried composite membranes with a length of 12 mm and an internal width of 2 mm were prepared and measured tensile strength using a universal electronic tester (Instron 3343, Instron, USA) at a speed of 20 mm min^{-1}. The same samples were immersed in saline for 2 h and wiped off the water on the surface. At the same condition, the tensile strength of the wet samples was also measured. The slope of the initial linear elastic portion of the stress–strain curve determines the elastic modulus.

2.4 *In vitro* analysis

2.4.1 Cell culture. MC3T3-E1 cells (Cellbank of Chinese Science Academy, China) were cultured in α-MEM (Gibco, USA) containing 10% FBS (Gibco, USA), 100 mg per mL streptomycin and 100 U per mL penicillin, and cultured with 5% CO_2 at 37 °C for subsequent cell tests.

2.4.2 Cell proliferation. The rounded composite membranes of each group were tailored for the size of 48-well plates and were sterilized by 75% ethanol and UV irradiation. Before cell culture, the membranes were immersed in the medium for prewetting for 2 h, and 100 μL of 3.0×10^4 cells per mL cell suspension was carefully dropped on the surface of each membrane and then placed in an incubator with 5% CO_2 at 37 °C for 1 h to ensure that the cells adhere to the surface of the materials. Subsequently, 200 μL of cell culture medium was added to each well. Cell proliferation was measured using a CCK-8 assay (Dojindo, Japan) every other day during the 7 day incubation starting on day 1.

2.4.3 Alkaline phosphatase (ALP) level and staining. The composite membranes were placed in 12-well plates, and 2.0×10^4 cells per well were seeded into each well. After the cell attachment, 50 μg per mL L-ascorbic acid (Beyotime, China), 10 mM sodium β-glycerophosphate (Beyotime, China), and 10^{-8} M dexamethasone (Beyotime, China) were added to the cell culture medium, and the solution was replaced every 3 days. After 7 and 14 days of culture, the cells in each group were stained with BCIP/NBT alkaline phosphatase staining kit (Beyotime, China). After washing with deionized water, the stain map was observed using an optical microscope (Leica, Germany). The concentration of *P*-nitrophenol and BCA protein in each group was measured using an alkaline phosphatase quantitative detection kit (Wako, Japan) and a BCA protein concentration determination kit (Beyotime, China). The experiment of each group was independently repeated at least three times.

2.4.4 Alizarin red staining. After 14 and 21 days of culture, the cells were fixed with 4% paraformaldehyde, rinsed with deionized water, and stained with 1 mL 40 mM Alizarin red for 15 min. An optical microscope (Leica, Germany) captured Alizarin red staining images.

2.4.5 Expression of osteogenesis-related genes. The MC3T3-E1 cells were plated on 6-well plates. After 24 h of incubation, the culture medium was replaced by osteogenic-inducing conditional medium. On days 14, total RNA from cells in different groups was extracted by TRIZOL reagent (Invitrogen, USA). With the housekeeping gene GAPDH serving as the internal reference, the expression levels of the mRNA-coding genes ALP, OSX, OPN, and RUNX2 were measured. The specific primer sequences (listed in Table S1†) were designed by Sangon Biotech (China) Co., Ltd.

2.5 Statistical analysis

Data were expressed as mean ± standard deviation. The statistical significance of the results was evaluated by one-way ANOVA analysis. $P < 0.05$ was considered statistically significant.

3. Results

3.1 Characterization of ACP nanoparticles and composite membranes

Stabilized ACP nanoparticles were prepared in an aqueous solution using ATP as a stabilizer. The ACP nanoparticles were uniformly dispersed in ethanol and observed by TEM, having a spherical structure and diameters of less than 20 nm (Fig. 1). Their amorphous nature was confirmed by selected area electron diffraction (SAED, Fig. 1). In addition, the ACP nanoparticles were further examined by SEM, whose contour is discernible, and subjected to elemental analysis by EDS, which detected the carbon derived from the ATP, confirming that the ATP interacts with ACP (Fig. 2a and b). The CCS–PVA and ACP–CCS–PVA composite membranes were fabricated through the freeze-drying process, and the internal structure was examined by SEM (Fig. 2c–f), where the hierarchical porous structure of mesoporous and macropore can be seen and also confirmed by N_2 adsorption–desorption isotherms (Fig. S1†). In addition, the calcium and phosphorus elements were evenly mixed with the

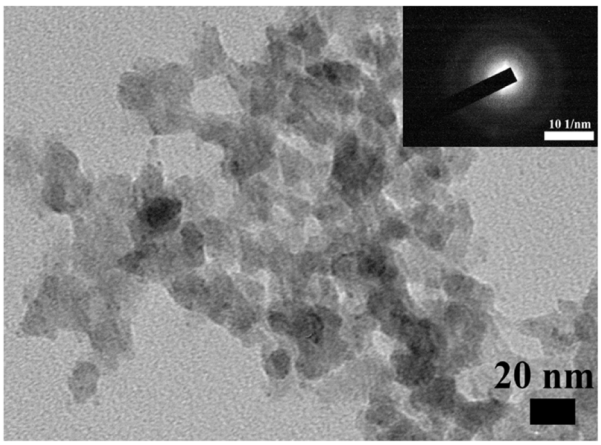

Fig. 1 TEM and SAED patterns of the ATP-stabilized ACP nanoparticles.

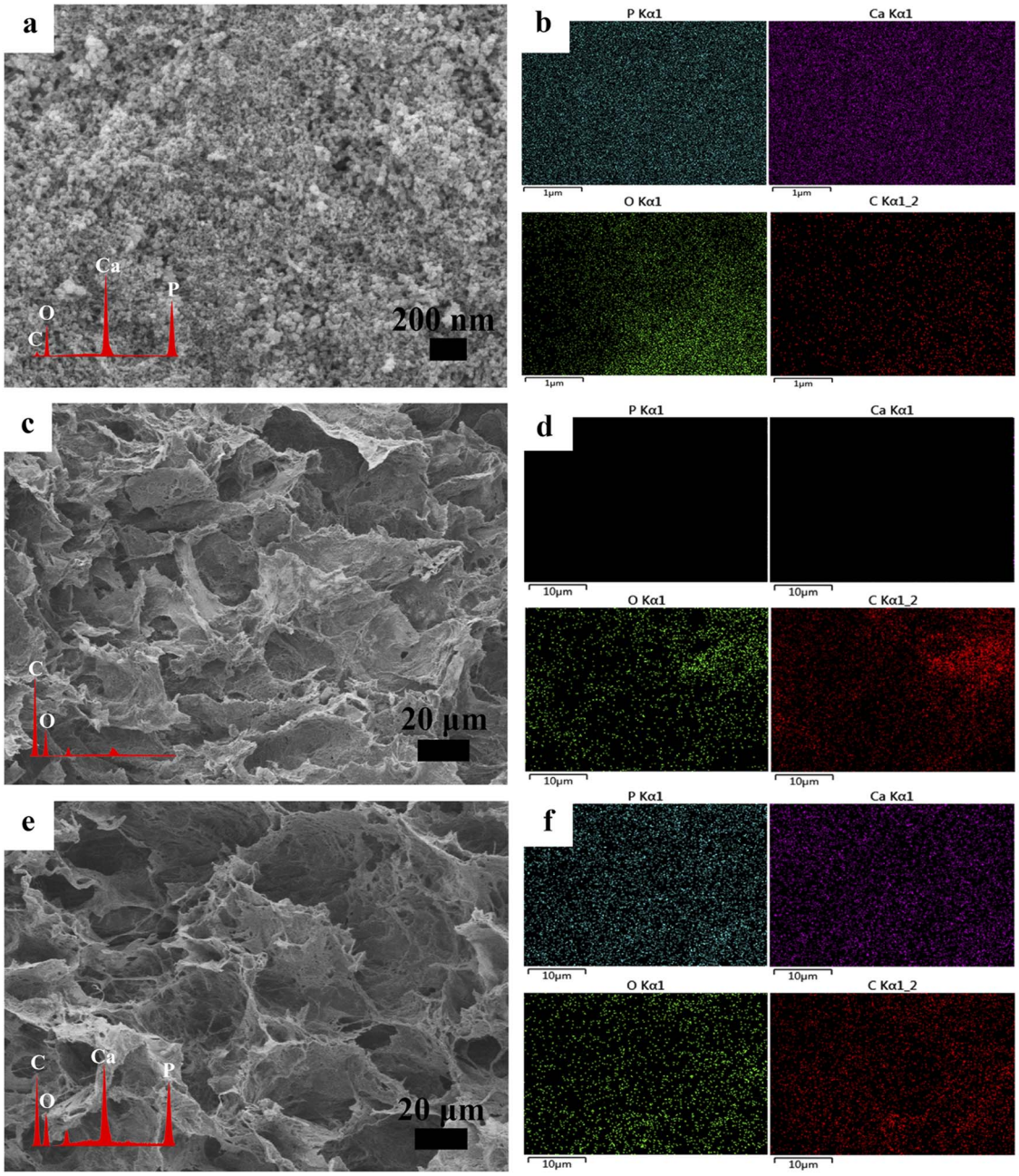

Fig. 2 (a) SEM of the ACP nanoparticles. (b) The EDS spectra show the element composition of ACP nanoparticles. (c) SEM of the CCS–PVA composite membrane. (d) The EDS spectra show the element composition of the CCS–PVA composite membrane. (e) SEM of the ACP–CCS–PVA composite membrane. (f) The EDS spectra show the element composition of the ACP–CCS–PVA composite membrane.

CCS and PVA, as shown by the EDS results, rather than aggregating together to form larger ACP particles.

The ACP nanoparticles and the composite membranes of CCS–PVA and ACP–CCS–PVA were examined using FTIR (Fig. 3a). Two characteristic peaks at 567 cm^{-1} and 1049 cm^{-1} appeared in ACP nanoparticles, attributed to the asymmetric bending vibration of P–O (ν_4) and the asymmetric stretching vibration of P–O (ν_1), respectively. The ν_4 peak of P–O blue shifted to 594 cm^{-1} implying that the ACP was successfully incorporated in the ACP–CCS–PVA composite membrane and confirmed that the ACP may interact with the CCS and PVA *via* a cation binding to carboxyl groups. However, the ν_1 peak of P–O was covered because the peak 1080 cm^{-1} arose from the C–O tensile vibration peak of PVA is too strong. In addition, a strong absorption peak arises at 1651 cm^{-1} in the ACP samples (Fig. S2†), attributed to the stretching vibration mode of the C=C group of the ATP,[31] indicating that the ATP interacts with ACP. Since the strong interaction, the ATP-stabilized ACP nanoparticles could be stabilized without phase change within 27 days when immersed in PBS solution at pH 7.4 (Fig. S3†). Furthermore, these materials were

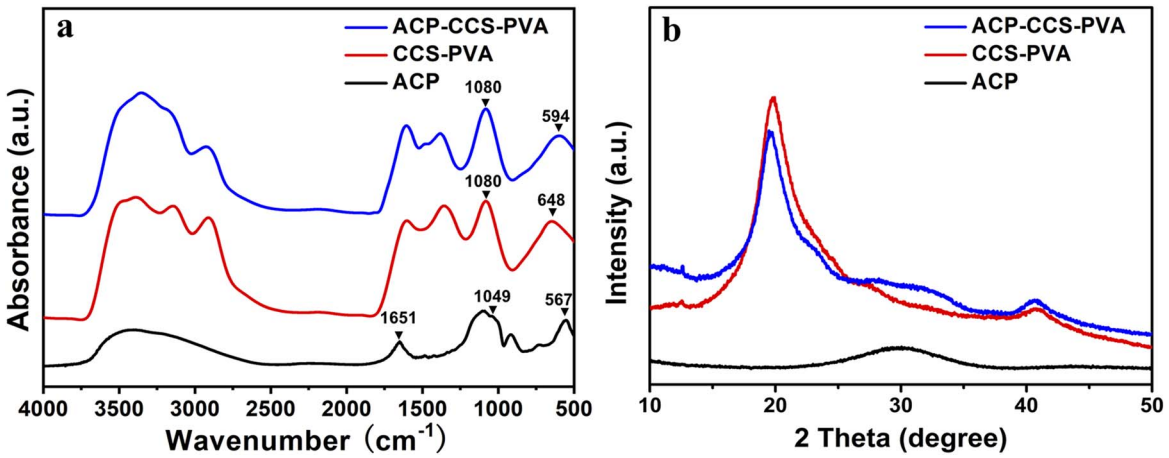

Fig. 3 (a) FTIR spectra and (b) XRD patterns of the ACP nanoparticles, the CCS–PVA composite membranes, and the ACP–CCS–PVA composite membranes.

further examined by XRD, where the broad peak at around two thetas of 30° suggested the amorphous nature of the mineral particles, and at around two thetas of 20° suggested that CCS–PVA was in the amorphous state (Fig. 3b).

3.2 Features of the composite membrane

3.2.1 Weight ratio of organic and inorganic analysis. The weight fraction of inorganic minerals in three types of composite membranes was determined by TGA. Initially, the weight loss occurred in the temperature range of 80–200 °C, mainly due to water evaporation. Subsequently, a weight loss was detected in the TGA curves in the temperature range of 200–600 °C because of the organic matter combustion. Therefore, the ratio of inorganic and organic could be calculated, which was 0 for CCS–PVA, 0.14 for 10 wt% ACP–CCS–PVA, and 0.30 for 20 wt% ACP–CCS–PVA (Fig. 4a).

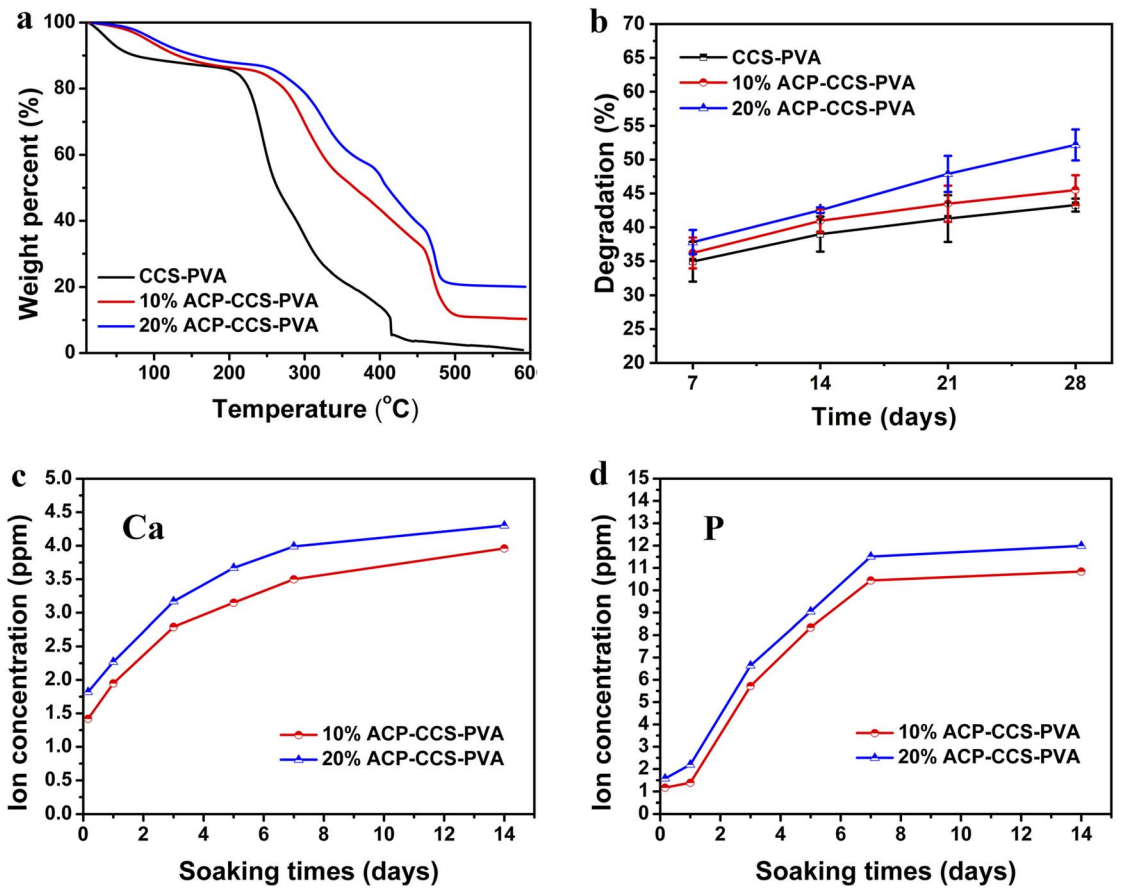

Fig. 4 (a) TGA curves, (b) degradation, (c) calcium ion, and (d) phosphate ion release curves of composite membranes.

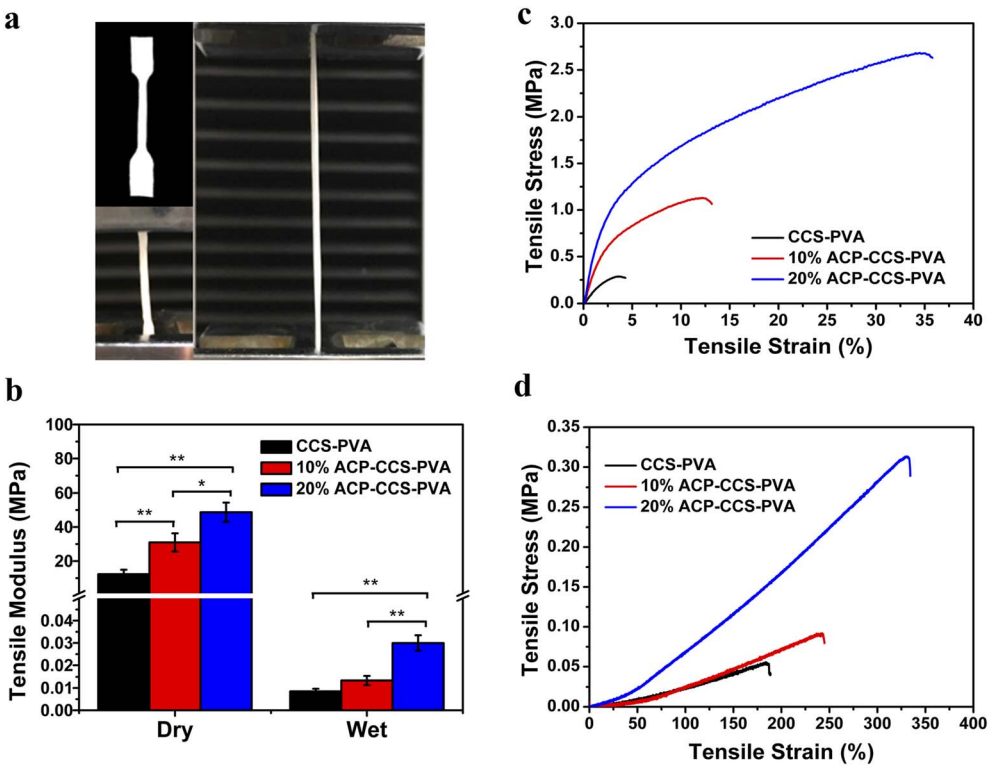

Fig. 5 (a) Mechanical properties testing device diagram. (b) Composite membranes' tensile modulus and stress–strain curves were obtained in (c) dry and (d) wet conditions (*$P < 0.05$, **$P < 0.01$, $n = 3$).

3.2.2 Degradation evaluation *in vitro*. The composite membranes were degraded in lysozyme-containing PBS buffer at 37 °C for 7, 14, 21, and 28 days (Fig. 4b) to assess the potential *in vivo* application. No significant difference was observed in these three groups during the 14 day degradation period. After 28 day degradation, the mass reduction was the greatest in the group of 20 wt% ACP–CCS–PVA (52.17 ± 2.27%) compared with the pure CCS–PVA (43.28 ± 0.96%) and 10 wt% ACP–CCS–PVA (45.5 ± 2.19%). It is a presumable reason that the ACP nanoparticles or released calcium and phosphate ions accelerated the activity of the lysozyme on organic matter.

3.2.3 The ion release of composite membranes. The inorganic ions would affect the differentiation and proliferation of cells such as mesenchymal stem cells,[32] and thus the release of calcium and phosphate ions from these composite membranes in saline was detected (Fig. 4c and d). Within 7 days, the concentration of calcium and phosphate ions increased progressively with the dissolution of the ACP. Over days 7 to 14, the concentration of two ions showed almost no change and reached a plateau stage. Compared with the 10 wt% ACP–CCS–PVA, the 20 wt% ACP–CCS–PVA material released more mineral ions.

3.2.4 Mechanical properties of composite membranes. Mechanical properties of a biomaterial play a crucial role in regulating the behavior of the cells in tissue engineering. Here, the composite membranes were examined in either dry or wet conditions. The composite membranes' tensile modulus (elastic modulus, E) was calculated from the stress–strain curves (Fig. 5b). The E of pure CCS–PVA, 10 wt%, and 20 wt% ACP–CCS–PVA composite membranes were 12.34 ± 2.58 MPa, 30.96 ± 5.35 MPa, and 48.69 ± 5.66 MPa, respectively, under dry condition. With the ACP content increasing, the E was dramatically enhanced, indicating that the ACP incorporated with the CCS and PVA could improve the mechanical properties of the organic membrane. However, these membranes' E became weaker in the wet state, and the values dropped to 0.009 ± 0.001 MPa, 0.013 ± 0.002 MPa, and 0.029 ± 0.003 MPa, respectively. These results were further confirmed by the stress–strain curves (Fig. 5c and d), where the 20 wt% ACP–CCS–PVA showed the most excellent deformation performance compared to the other groups, whether in dry or wet conditions. These findings echos the previous results that organic-inorganic composite materials have a better mechanical performance than pure organic materials, especially for boosting strength.

3.3 Biological behavior of composite membranes

3.3.1 Cell proliferation. The proliferation of MC3TC-E1 cells on the composite membranes was tested through the CCK8 assay (Fig. 6a). The absorbance at 450 nm of each sample was recorded at 1, 3, 5, and 7 days. On day 1, there was no statistically significant difference in cell proliferation in the three groups. From day 3, the ability of the ACP–CCS–PVA composite membrane to promote cell proliferation was greater than that of the CCS–PVA, suggesting the ACP could improve the interaction between organic material and cells, possibly through mechanical properties or mineral ion release. In

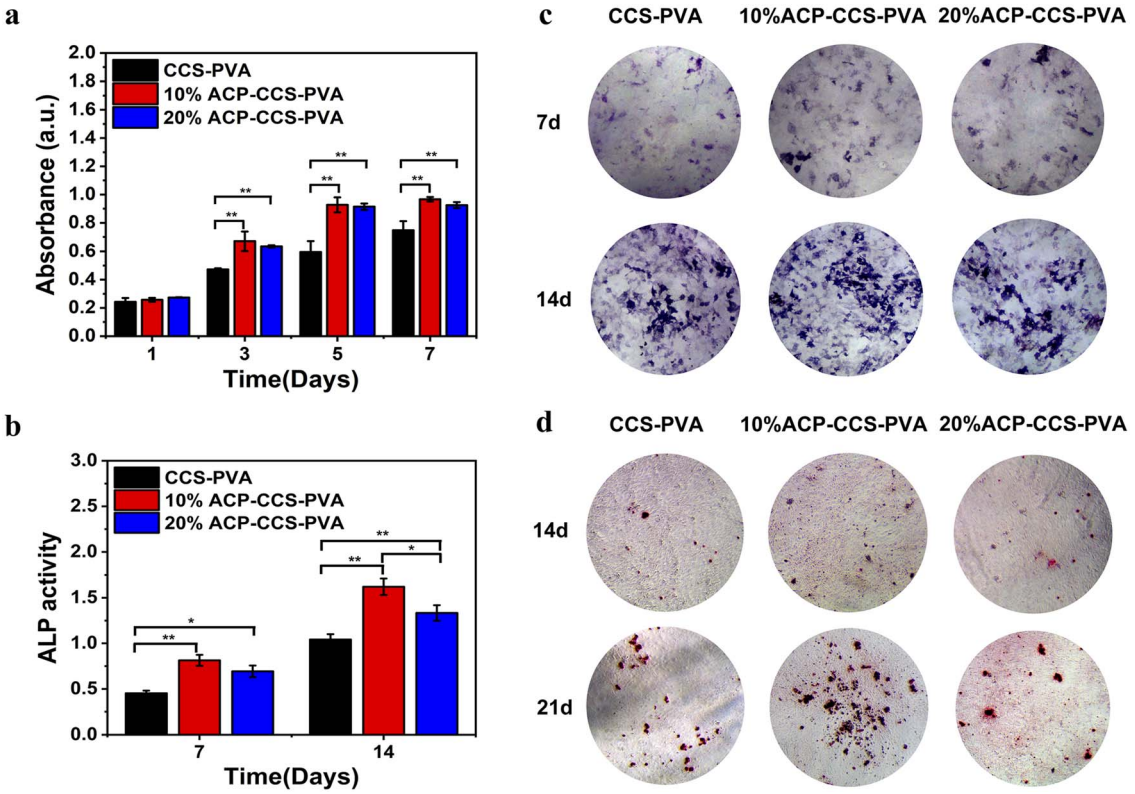

Fig. 6 (a) CCK-8 assay results of CCS–PVA, 10 wt%, and 20 wt% ACP–CCS–PVA composite membranes. The ALP activity (b) and staining (c) were on the 7th and 14th days. (d) The alizarin red staining was on the 14th and 21st days (*P < 0.05, **P < 0.01, n = 3).

addition, mouse fibroblasts (L929) were co-cultured with the composite membranes, and the results showed that all the cells on the composite membranes had a survival rate of more than 75%, with good biocompatibility and no cytotoxicity (Fig. S6†).

3.3.2 Inducing osteogenesis *in vitro*. The ALP activity signals the osteogenic differentiation of cells, which could evaluate biomaterial efficiency for bone tissue repair. In the present study, we detected the ALP activity in the MC3T3-E1 cells, which culture on the surface of the composite membrane. The ALP activity of MC3T3-E1 was evaluated through qualitative and quantitative analysis after 7 and 14 days (Fig. 6b and c and S4†). With time prolonged, the ALP activity becomes stronger in three groups. The ALP staining and ALP activity measurement show that the ACP–CCS–PVA has a higher level than the pure CCS–PVA.

Furthermore, alizarin red staining was conducted on the 14th and 21st days to further assess composite membranes' capacity to promote osteogenesis (Fig. 6d). The 10 wt% ACP–CCS–PVA can effectively stimulate the mineralization nodules formation compared with the CCS–PVA and 20 wt% ACP–CCS–PVA.

The transcription levels of osteogenic genes on days 14 were presented in Fig. 7, and those of osteogenic genes in the 10 wt% ACP–CCS–PVA group were significantly increased compared with the CCS–PVA and 20 wt% ACP–CCS–PVA groups. These results demonstrate osteogenic differentiation of cells, whereas excess ACP could suppress cell differentiation.

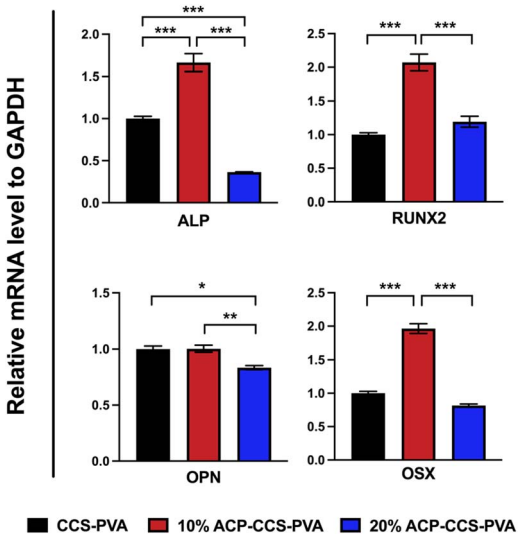

Fig. 7 The mRNA expression of osteogenesis-related genes was analyzed after incubated for 14 days (*P < 0.05, **P < 0.01, ***P < 0.001, n = 3).

4. Discussion

Numerous studies have demonstrated that using GBR membranes can improve bone formation,[33–35] but rather than focusing on the cellular and molecular mechanisms of GBR,

researchers have mainly studied the histological assessment of bone formation under the membrane cover. The mechanism is currently thought to be that GBR membranes act as a passive barrier to soft tissue invasion while ignoring their fundamental role in promoting bone regeneration.[36] Some studies suggest that the GBR membranes stimulate the local environment in the bone defect area, which is beneficial for the recruitment and differentiation of various cell types, including osteoblasts and osteoclasts.[37] These findings accelerate understanding of the mechanism by which GBR membranes promote bone regeneration and the manufacture and application of new biomaterials.

In the present study, we fabricated an organic–inorganic composite membrane, which could serve as a barrier membrane for the potential application of GBR. Pure ACP is unstabilized in an aqueous solution and quickly transforms into thermodynamically more stable HAP crystals.[38] Therefore, a biomolecule, ATP, was used here to stabilize ACP for a long time (in our case, we could stabilize it for 27 days; see Fig. S3†). Then we could directly investigate how ACP affects the cell behavior rather than crystallizing calcium phosphate. The organic components are CCS and PVA, which could form a strong network structure by forming hydrogen bonds between the hydroxyl groups of PVA and the carboxyl groups of CCS.[39] When ACP is incorporated into the CCS and PVA system, there is an interaction between the mineral and organic matter through the binding of calcium to carboxyl groups, which enhances the mechanical performance of ACP–CCS–PVA compared to the pure CCS–PVA membrane. Due to the biological material's open porosity and excellent hydrophilicity, the ACP–CCS–PVA composite membrane produced a rigid and elastic hydrogel state, particularly in wet conditions similar to body fluids. These properties are consistent with a suitable biomaterial that could provide a well-matched mechanical microenvironment of the extracellular matrix, which is critical in regulating cell adhesion, migration, proliferation, and differentiation.[40] In our case, the ACP–CCS–PVA composite membrane's higher elastic modulus might activate the cells' mechanical signaling pathway and effectively promote the osteogenic differentiation of cells. Although the swelling curves reflected that the incorporation of ACP made the ACP–CCS–PVA composite membranes denser in structure (Fig. S5†), they still have good pore structure, and the good pores can promote the diffusion of liquid, oxygen, and bioactive substances.[41]

The evaluation of the osteogenesis of the composite membrane shows that the ACP–CCS–PVA membranes are more robust than the CCS–PVA, and 10 wt% ACP incorporation is optimal, rather than the ACP amount higher and better. The slow, continuous release of calcium and phosphate ions from ATP-stabilized ACP nanoparticles not only selectively binds serum proteins and integrin receptors but also attracts osteoblasts, improving the microenvironment for bone formation.[42,43] In addition, ACP may act as a calcium and phosphate reservoir to promote the mineral deposition in collagen fibrils, a significant component of bone. These factors suggest that calcium phosphate minerals may improve bone formation to some extent through chemical and biological pathways. Nevertheless, we discovered that the amount of ACP added to the composite membrane was not proportionate to the enhancement of osteogenic differentiation of MC3T3-E1 cells by ALP activity assay, alizarin red staining assay (Fig. 6b–d) and expression of osteogenic genes (Fig. 7). Because excess ACP is thought to cause excessive ion release, and local high ion concentrations interfere with related signaling pathways in osteoblasts, thereby affecting bone metabolism.[44] For example, ACP NPs/macrophage-modulated environments attenuated the osteogenic capacity of BMSCs,[45] sustained calcium ions in bone-forming solutions facilitated osteogenic differentiation of the cells, and ACP in its non-crystalline state was susceptible to transformation into HAP, which induced a decrease in calcium concentration leading to downregulation of the expression of osteogenesis-related proteins.[46] Therefore, the ATP-stabilised ACP in this study can continuously release calcium and phosphate ions, which is considered to be a factor for increasing ALP activity, but whether the high concentration of ACP is a potential inflammatory factor in the process of cellular osteogenic differentiation also needs to be further investigated.

5. Conclusions

In conclusion, we found that ACP–CCS–PVA composite membranes have improved mechanical properties and promoted osteogenic differentiation of cells compared to CCS–PVA composite membranes, demonstrating their great potential in GBR. Although a higher ACP content has a superior mechanical strength, the excess ACP would negatively influence cell proliferation and osteogenic differentiation. Further research is required to investigate *in vivo* effect of the ACP–CCS–PVA composite membranes and their molecular mechanism for guiding bone tissue regeneration. These findings highlight the significant role of calcium phosphate in bone regeneration and provide a strategy for biomaterial preparation to balance the mechanical properties and mineral content.

Author contributions

Qiaolin Du and Jian Sun: methodology, investigation, writing – original draft, writing – review & editing. Yanyan Zhou: investigation, formal analysis. Yadong Yu: validation. Weijing Kong: project administration. Chaoqun Chen: funding acquisition. Yifeng Zhou and Ke Zhao: software. Changyu Shao: conceptualization, supervision, writing – review & editing. Xinhua Gu: conceptualization, supervision, funding acquisition, methodology, writing – review & editing.

Conflicts of interest

There are no conflicts to declare.

Acknowledgements

This work was supported by the Medical Health Science and Technology Project of Zhejiang Provincial Health Commission (grant no. 2023KY092) and the Research and Development

Project of Stomatology Hospital Zhejiang University School of Medicine (grant no. RD2022JCYL07).

References

1 J. I. Sasaki, G. L. Abe, A. Li, P. Thongthai, R. Tsuboi, T. Kohno and S. Imazato, *Biomater. Invest. Dent.*, 2021, **8**, 54–63.
2 J. Caballe-Serrano, Y. Abdeslam-Mohamed, A. Munar-Frau, M. Fujioka-Kobayashi, F. Hernandez-Alfaro and R. Miron, *Arch. Oral Biol.*, 2019, **100**, 57–68.
3 S. Jin, J. Li, J. Wang, J. Jiang, Y. Zuo, Y. Li and F. Yang, *Int. J. Nanomed.*, 2018, **13**, 4591–4605.
4 A. R. Padalhin, N. Thuy Ba Linh, Y. Ki Min and B. T. Lee, *J. Biomater. Sci., Polym. Ed.*, 2014, **25**, 487–503.
5 Y. Tu, C. Chen, Y. Li, Y. Hou, M. Huang and L. Zhang, *Bio-Med. Mater. Eng.*, 2017, **28**, 223–233.
6 F. Han, P. Zhang, Y. Sun, C. Lin, P. Zhao and J. Chen, *Int. J. Nanomed.*, 2015, **10**, 7333–7343.
7 N. Eliaz and N. Metoki, *Materials*, 2017, **10**, 334.
8 D. Ege, Q. Nawaz, A. M. Beltran and A. R. Boccaccini, *ACS Biomater. Sci. Eng.*, 2022, **8**, 5273–5283.
9 D. Ege, K. Zheng and A. R. Boccaccini, *ACS Appl. Bio Mater.*, 2022, **5**, 3608–3622.
10 W. C. Lepry and S. N. Nazhat, *Adv. NanoBiomed Res.*, 2021, **1**, 2000055.
11 M. Schweikle, S. H. Bjornoy, A. T. J. van Helvoort, H. J. Haugen, P. Sikorski and H. Tiainen, *Acta Biomater.*, 2019, **90**, 132–145.
12 S. Gorodzha, T. E. Douglas, S. K. Samal, R. Detsch, K. Cholewa-Kowalska, K. Braeckmans, A. R. Boccaccini, A. G. Skirtach, V. Weinhardt, T. Baumbach, M. A. Surmeneva and R. A. Surmenev, *J. Biomed. Mater. Res., Part A*, 2016, **104**, 1194–1201.
13 G. Balasundaram, M. Sato and T. J. Webster, *Biomaterials*, 2006, **27**, 2798–2805.
14 D. Tadic, F. Peters and M. Epple, *Biomaterials*, 2002, **23**, 2553–2559.
15 B. M. Whited, D. Skrtic, B. J. Love and A. S. Goldstein, *J. Biomed. Mater. Res., Part A*, 2006, **76**, 596–604.
16 G. F. Smaisim, K. J. Mohammed, S. K. Hadrawi, H. Koten and E. Kianfar, *Bionanoscience*, 2023, **13**, 819–839.
17 Z. S. Abbas, M. M. Kadhim, A. M. Rheima, A. D. J. Al-bayati, Z. T. Abed, F. M. D. Al-Jaafari, A. S. Jaber, S. K. Hachim, Z. H. Mahmoud, F. K. Ali, H. Koten and E. Kianfar, *Bionanoscience*, 2023, **13**, 983–1011.
18 A. Taloni, M. Vodret, G. Costantini and S. Zapperi, *Nat. Rev. Mater.*, 2018, **3**, 211–224.
19 S. Yao, X. Lin, Y. Xu, Y. Chen, P. Qiu, C. Shao, B. Jin, Z. Mu, N. Sommerdijk and R. Tang, *Adv. Sci.*, 2019, **6**, 1900683.
20 J. S. Martinez, T. C. Keller 3rd and J. B. Schlenoff, *Biomacromolecules*, 2011, **12**, 4063–4070.
21 Y. Ren, L. Fan, S. Alkildani, L. Liu, S. Emmert, S. Najman, D. Rimashevskiy, R. Schnettler, O. Jung, X. Xiong and M. Barbeck, *Int. J. Mol. Sci.*, 2022, **23**, 14987.
22 C. Chu, J. Deng, X. Sun, Y. Qu and Y. Man, *Tissue Eng., Part B*, 2017, **23**, 421–435.
23 M. Ahmadipour, H. Mohammadi, A. L. Pang, M. Arjmand, T. A. Otitoju, P. U. Okoye and B. Rajitha, *Int. J. Polym. Mater. Polym. Biomater.*, 2022, **71**, 180–195.
24 S. Chen, H. Tian, J. Mao, F. Ma, M. Zhang, F. Chen and P. Yang, *Int. J. Biol. Macromol.*, 2023, **226**, 410–422.
25 D. T. Wu, J. G. Munguia-Lopez, Y. W. Cho, X. Ma, V. Song, Z. Zhu and S. D. Tran, *Molecules*, 2021, **26**, 7043.
26 O. Kamaci, N. Yucel, H. Koten, E. Bulus and G. S. Bulus, *J. Polytech.*, 2023, **1**, 1.
27 J. M. Unagolla, T. E. Alahmadi and A. C. Jayasuriya, *Carbohydr. Polym.*, 2018, **199**, 426–436.
28 K. Hozumi and M. Nomizu, *Int. J. Mol. Sci.*, 2018, **19**, 2713.
29 D. Coelho, A. Sampaio, C. J. S. M. Silva, H. P. Felgueiras, M. T. P. Amorim and A. Zille, *ACS Appl. Mater. Interfaces*, 2017, **9**, 33107–33118.
30 M. J. Pei, D. Zhu, J. F. Yang, K. D. Yang, H. J. Yang, S. J. Gu, W. Q. Li, W. L. Xu, P. Xiao and Y. S. Zhou, *Eur. Polym. J.*, 2023, **182**, 111737.
31 C. Qi, Y. J. Zhu, B. Q. Lu, X. Y. Zhao, J. Zhao, F. Chen and J. Wu, *Small*, 2014, **10**, 2047–2056.
32 A. Ressler, M. Antunovic, L. Teruel-Biosca, G. G. Ferrer, S. Babic, I. Urlic, M. Ivankovic and H. Ivankovic, *Carbohydr. Polym.*, 2022, **277**, 118883.
33 G. I. Benic, D. S. Thoma, F. Munoz, I. Sanz Martin, R. E. Jung and C. H. Hammerle, *Clin. Oral Implants Res.*, 2016, **27**, 567–576.
34 S. Pajoumshariati, H. Shirali, S. K. Yavari, S. N. Sheikholeslami, G. Lotfi, F. Mashhadi Abbas and A. Abbaspourrad, *Sci. Rep.*, 2018, **8**, 7513.
35 M. Lian, B. Sun, Z. Qiao, K. Zhao, X. Zhou, Q. Zhang, D. Zou, C. He and X. Zhang, *Colloids Surf., B*, 2019, **176**, 219–229.
36 I. Elgali, O. Omar, C. Dahlin and P. Thomsen, *Eur. J. Oral Sci.*, 2017, **125**, 315–337.
37 O. Omar, I. Elgali, C. Dahlin and P. Thomsen, *J. Clin. Periodontol.*, 2019, **46**, 103–123.
38 S. V. Dorozhkin, *Biomater. Sci.*, 2021, **9**, 7748–7798.
39 L. Nie, Y. Deng, P. Li, R. Hou, A. Shavandi and S. Yang, *ACS Omega*, 2020, **5**, 10948–10957.
40 N. Alcorta-Sevillano, I. Macias, A. Infante and C. I. Rodriguez, *Cells*, 2020, **9**, 2630.
41 P. Xia and Y. Luo, *J. Biomed. Mater. Res., Part B*, 2022, **110**, 1206–1214.
42 W. He, M. Andersson, P. P. de Souza, C. A. de Souza Costa, E. M. Munoz, H. O. Schwartz-Filho, M. Hayashi, A. Hemdal, A. Fredel, A. Wennerberg and R. Jimbo, *Biomed. Mater.*, 2013, **8**, 035007.
43 X. Niu, S. Chen, F. Tian, L. Wang, Q. Feng and Y. Fan, *Mater. Sci. Eng., C*, 2017, **70**, 1120–1124.
44 P. Berube, Y. Yang, D. L. Carnes, R. E. Stover, E. J. Boland and J. L. Ong, *J. Periodontol.*, 2005, **76**, 1697–1709.
45 L. Chen, P. Qiao, H. Liu and L. Shao, *Inflammation*, 2021, **44**, 278–296.
46 O. Groninger, S. Hess, D. Mohn, E. Schneider, W. Stark, S. Marsmann, P. Wolint, M. Calcagni, P. Cinelli and J. Buschmann, *Int. J. Mol. Sci.*, 2020, **21**, 2627.